

Constraints on SN Ia progenitor time delays from high-*z* SNe and the star-formation history

F. Forster^{1?}, C. W. Olf¹, Ph. Podsiadlowski^{1,z}, Z. Han^{2,x}

¹Dept. of Physics, University of Oxford, Denys Wilkinson Building, Keble Road, Oxford, OX1 3RH, United Kingdom

²National Astronomical Observatories/Yunnan Observatory, the Chinese Academy of Sciences, P.O. Box 110, Kunming, 650011, China

Accepted 2006 March 01. Received 2006 February 28; in original form 2006 January 19

ABSTRACT

We re-assess the question of a systematic time delay between the formation of the progenitor and its explosion in a type Ia supernova (SN Ia) using the Hubble Higher-*z* Supernova Search sample (Strolger et al. 2004). While the previous analysis indicated a significant time delay, with a most likely value of 3.4 Gyr, effectively ruling out all previously proposed progenitor models, our analysis shows that the time-delay estimate is dominated by systematic errors, in particular due to uncertainties in the star-formation history. We find that none of the popular progenitor models under consideration can be ruled out with any significant degree of confidence. The inferred time delay is mainly determined by the peak in the assumed star-formation history. We show that, even with a much larger supernova sample, the time delay distribution cannot be reliably reconstructed without better constraints on the star-formation history.

Key words: supernovae: general | cosmology: observational

1 INTRODUCTION

Type Ia supernovae have been used extensively as standard distance indicators and have provided the best evidence to date for an acceleration of the Universe (Riess et al. 1998; Perlmutter et al. 1999; Riess et al. 2004). Future missions, e.g. GAIA and SNAP, will greatly increase the number of detected SNe Ia and significantly reduce the statistical errors in the determination of cosmological parameters. However, the nature of the progenitors of type Ia supernovae is still unknown and the empirically calibrated Phillips relation (Phillips 1993) is not fully understood physically.

Several progenitor scenarios are under discussion, but there is no consensus due to uncertainties in the evolutionary processes (Hachisu & Nomoto 1996; Hachisu et al. 1999; Li & van den Heuvel 1997; Langer et al. 2000; Han & Podsiadlowski 2004) and the explosion mechanism (Hillebrandt & Niemeyer 2000; Röpke & Hillebrandt 2005; Gametzko Khokhlov & Oran 2005). One of the signatures of the various scenarios is the distribution of time delays between the formation of the progenitor systems and their explosion, which could give rise to a significant difference be-

tween the redshift dependence of the supernova rate (SNR) and the star-formation history (SFH).

Strolger et al. (2004), hereafter S04, aimed to detect this difference by studying the distribution of 25 high-*z* SNe Ia in the Hubble Higher-*z* Supernova Search sample (Riess et al. 2004). Their approach was to infer the mean time delay of the distribution using a Bayesian analysis, which assumed different parametrized time-delay distributions and adopted the star-formation history (SFH) from Giallisco et al. (2004), hereafter G04. They concluded that mean time delays shorter than 2 Gyr ought to be excluded with a 95 per cent confidence level, ruling out essentially all progenitor scenarios currently under discussion. In a recent re-assessment of the constraints, Strolger et al. (2005b) obtained a 95 per cent lower limit ranging from 0.2 to 1.6 Gyr for different time-delay distributions. In the corrected best-fitting model, the 95 per cent confidence interval ranged from 1 to 4.4 Gyr with the most likely value at 3.4 Gyr.

Unlike core collapse SNe (SNe II, Ib/c) that originate from massive progenitors with relatively short main-sequence (MS) lifetimes (~ 3 – 20 Myr), SNe Ia are believed to be thermonuclear explosions of white dwarf stars (WDs) whose progenitors have MS lifetimes ranging from ~ 30 Myr to several billion years. This implies a minimum time delay for SNe Ia of the order of ~ 30 Myr.

Most of the SN Ia progenitor scenarios that have been proposed involve mass transfer on to a CO WD in a binary system, either through the expansion and Roche lobe over-

? fix@astro.ox.ac.uk

y cwo@astro.ox.ac.uk

z podsi@astro.ox.ac.uk

x zhanwen@public.km.cn

ow of an evolved companion (single degenerate [SD] scenarios) or through the slow release of gravitational waves, orbital shrinking, Roche lobe overflow and merging of a compact double WD system (double-degenerate [DD] scenarios). Both scenarios have associated time-delay distributions that have been estimated with binary population synthesis codes (BPS), where the properties of binary systems are followed from their birth up to the explosion stage through their many different evolutionary paths. Independently of the particular treatment of the binary interactions, the resulting time-delay distributions differ considerably since their characteristic time-scales have different origins.

The SD scenario is controlled by the process of mass accretion, which has to occur at just the correct critical rate in order to allow the growth of the mass of the companion WD up to the Chandrasekhar limit (Nomoto & Kondo 1991). The dominant evolutionary path seems to occur via the accretion of matter on to a CO WD from a slightly evolved MS star, the CO WD + MS { SD scenario (van den Heuvel et al. 1992; Rappaport, DiStefano, & Smith 1994; Li & van den Heuvel 1997; Langer et al. 2000; Han & Podsiadlowski 2004). In this channel, the accretion rate is determined mainly by the mass of the donor star, which must lie in a narrow range in order to satisfy the required accretion-rate constraints. As a consequence, the distribution of MS lifetimes and the time-delay distribution of the channel are relatively narrow, peaking at ~ 670 Myr and rapidly becoming negligible after 1.5 Gyr.

Although recent simulations have suggested that other evolutionary paths within the SD framework are of minor importance (Han & Podsiadlowski 2004), it is quite possible that their contribution has been underestimated. This is particularly important for the CO WD + RG { SD scenario, where a red-giant (RG) star accretes matter on to a CO WD star (Hachisu & Nomoto 1996); in this channel the time-delay distribution extends up to several Gyr.

The DD scenario (Iben & Tutukov 1984; Webbink 1984), in contrast, is controlled by the time that it takes for the binary system to coalesce, which depends roughly on the fourth power of the separation of the double-degenerate system (Shapiro & Teukolsky 1983). As a result, the time-delay distribution can be described by a low time-delay cutoff (~ 30 – 100 Myr) and an approximately power-law decline up to the age of the Universe. The lower time-delay cutoff can be explained by the time required to form the most massive degenerate systems with the shortest MS lifetimes, whereas the power-law tail can be explained by the power-law relation between coalescence time and separation of the double-degenerate systems.

However, the expected accretion rates in the DD scenario are a problem: they are so high that present calculations suggest that this leads to accretion-induced collapse (AIC) and the formation of a compact object rather than a thermonuclear explosion (Nomoto & Iben 1985; Saio & Nomoto 1985, 1998; Timmes, Woosley, & Taam 1994; Nomoto & Kondo 1991).

Therefore, the currently generally most favoured progenitor scenario is the SD scenario. Because the seemingly dominant evolutionary path of this channel would need to be discarded if the mean time-delay were found to be higher than 2 Gyr, it is important to confirm the significance of the S04 results.

In this work we have studied the SNe Ia time-delay distribution using the sample of S04 and the same basic analysis, but introducing alternative SFHs found in the literature, avoiding binning effects as much as possible and using a Goodness of Fit (GoF) test that is generally recommended for small samples. We discuss the data and analysis in Section 2, show the results and Monte Carlo simulations in Sections 3 and 4 and discuss their significance in Sections 5 and 6. Throughout this paper, we adopted a value for the Hubble constant of $H_0 = 70 \text{ km s}^{-1} \text{ Mpc}^{-1}$, present ratios of matter, curvature and dark energy density over the critical density of $\Omega_m = 0.3$, $\Omega_K = 0$ and $\Omega_\Lambda = 0.7$, respectively, and a 'dark energy' pressure over density ratio ('equation of state') of $w = -1$.

2 DATA AND ANALYSIS

The analysis is based on the Hubble Higher- z Supernova Search sample (Riess et al. 2004; Dahlen et al. 2004; Strolger et al. 2004), which contains 25 SNe Ia found in the GOODS field (13 in the Hubble Deep Field North, HDFN, and 12 in the Chandra Deep Field South, CDFS) in the redshift range 0.21 to 1.55. The SNe were discovered in four difference images that were produced by observing both fields *ve* times in intervals of approximately one month, comparable to the typical duration of the main SNe Ia light curve peak.

To infer the underlying time-delay distribution of SNe Ia, S04 compared the observed redshift distribution in the sample with a parametrized predicted distribution, derived from the G04 SFH convolved with three alternative time-delay distributions.

Each distribution was parametrized by its mean time delay, which was recovered using a Bayesian analysis. Among these, the distribution that best fit the data was a 'narrow Gaussian', which after being corrected was centred on 3.4 Gyr with a FWHM of ~ 1.5 Gyr. The 95 per cent confidence interval for the mean time delay ranged from 1.0 to 4.4 Gyr. The alternatives 'wide Gaussian' and 'folding distributions' had a mean time delay above 0.2 and 1.6 Gyr, respectively, with more than 95 per cent confidence.

Only the shapes of the distributions are compared, i.e. the analysis is scale-free, and the associated efficiencies of SNe per unit formed mass are calculated later by normalising the models to the SN numbers and are not used to constrain the models. This means that the sample must ideally span a redshift range that includes both the rising and declining parts of the SNR, i.e. where the SNR is not approximately linear. A recent study (see Barris & Tonry 2005, Fig. 6(8)) could not fully exploit information on the SN redshift distribution because their sample did not reach to a sufficiently high redshift ($z > 1$), as the authors indicate in the text. A similar situation is found in the work of Gal-Yam & Maoz (2004).

Thus, because the Hubble Higher- z Supernova Search sample is the deepest SN sample available, it is the most suitable one for constraining the time-delay distribution of SNe Ia.

However, the formal errors quoted in S04 reflect only the limited size of the sample and not other systematic uncertainties, such as those associated with the SFH.

In the following Sections 2.1 to 2.3 we introduce the for-

malism that gives the SNR, the number of detected SNe per unit redshift and the control times used in the derivations. In Section 2.4 we discuss alternative time-delay distributions and in Section 2.5 alternative SFHs. The Bayesian analysis is described in Section 2.6 and further modifications concerning binning effects and the GOF test are discussed in Section 2.7.

2.1 The SN Ia rate

The rate of SNe Ia per unit time per unit comoving volume (SNR_{Ia}) is given by the star-formation rate per unit time per unit comoving volume (SFH) convolved with the normalised distribution of explosions per unit time of the progenitor channel (the time-delay distribution, τ), and multiplied by the number of SNe per unit formed mass (the efficiency, ϵ). We assume that neither ϵ nor τ evolve with redshift:

$$\text{SNR}_{\text{Ia}}(z) = \int_{t(z_R)}^{t_0} \text{SFH}(t^0) \tau(t^0 - t; \tau) dt^0; \quad (1)$$

where $t = t(z)$, is some characteristic time-scale defined in Section 2.4 and z_R is the redshift associated with the time when the first stars formed, approximately the epoch of reionisation. We assumed $z_R = 10$, as in S04.

2.2 Distribution of detected SNe

The number of detected SNe Ia per unit redshift interval (n_{Ia}) is given by the multiplication of the rate of SNe Ia per unit time per unit comoving volume (SNR_{Ia}), a time dilation factor, $(1+z)^{-1}$, the control time of the survey (t_c) and the volume per unit redshift being surveyed, $\frac{dV}{dzd!}$:

$$n_{\text{Ia}}(z) = \frac{\text{SNR}_{\text{Ia}}(z)}{1+z} t_c(z) \frac{dV(z)}{dzd!}; \quad (2)$$

where in our cosmology the volume derivative formula simplifies to:

$$\frac{dV}{dzd!} = d_c^2 \frac{d(d_c)}{dz}, \text{ where} \quad (3)$$

$$d_c = c H_0^{-1} \int_0^z du (1+u)^3 M + \dots^{1=2}; \quad (4)$$

and hence,

$$\frac{dV(z)}{dzd!} = c H_0^{-1} (1+z)^3 M + \dots^{1=2} d_c^2(z); \quad (5)$$

2.3 The control time

The control time can be understood as the total observing time multiplied by the probability of detecting a SN at a given redshift. We used the same values as S04, that were calculated taking into account the expected extinction, spectra, light curve shapes and peak magnitude dispersion of SNe Ia, the way each field was revisited, and the efficiency of the detection algorithm (but see Section 2.7.1). The control times are defined by

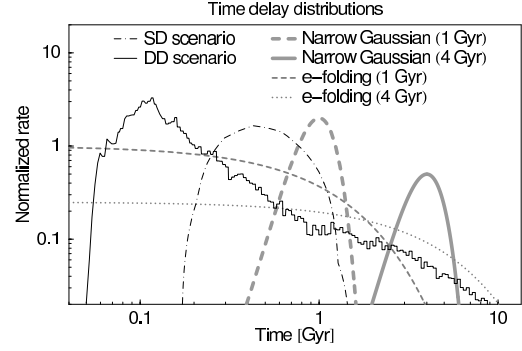


Figure 1. Theoretical time delay distributions (Han & Podsiadlowski 2004) compared to parametrized time delay distributions used in the analysis. The best-fitting model in S04 corresponds to the 'narrow Gaussian' distribution with a mean time delay of 4 Gyr.

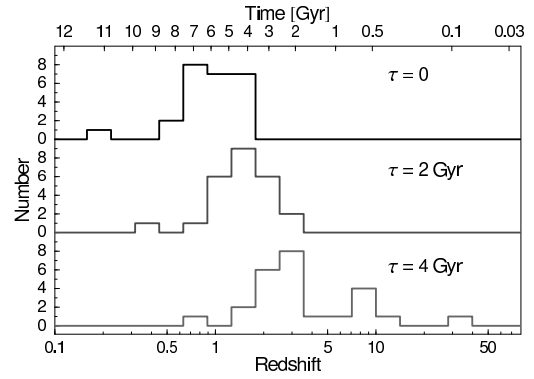


Figure 2. Histogram of progenitor formation redshifts for the 25 SNe in the Hubble Higher-z Supernova Search sample assuming unique time delays. Note that some SN progenitors must have originated at extremely high redshifts if the time delays were always high.

$$t_c(z) = \int_{t_0}^{t_c} P(t; M; A; z) P(M) P(A) dM dA dt; \quad (6)$$

where $P(t; M; A; z)$ is the probability of detecting a new SN at time t , given its rest-frame luminosity and its host galaxy extinction and redshift. It depends on the assumed spectra through K corrections, the sensitivity of the survey and the efficiency of the detection algorithm.

$P(M)$ is the probability of having a given SN rest-frame luminosity. It was estimated based on the characteristic relation between peak luminosity and light curve shape of SNe, and the observed dispersion of SN Ia peak luminosities.

$P(A)$ is the probability of having a given host galaxy extinction at the given rest-frame wavelength. It was assumed to be proportional to e^{-A} .

For more details see the original discussion in S04.

2.4 Time delay distributions

All the time delay distributions were parametrized by their mean time delays, τ . S04 used an exponential distribution

and two families of Gaussian distributions whose width scale with the mean time delay. The ϵ -folding distributions are given by:

$$(t; \epsilon) = \frac{e^{-t/\epsilon}}{\epsilon} : \quad (7)$$

The two alternative Gaussian distributions are grouped into the families of 'narrow' ($\epsilon = 0.2$) and 'wide' ($\epsilon = 0.5$) distributions, of the form:

$$(t; \epsilon) = \frac{1}{\epsilon \sqrt{2\pi}} e^{-\frac{(t-\epsilon)^2}{2\epsilon^2}} : \quad (8)$$

The previous distributions are defined only for positive values. However, negative time delays must be allowed in order to avoid statistical bias in a small sample and to get confidence intervals that do not artificially discard short time delays. Moreover, a preference for negative time delays would signal SFHs that peak too late in time. Thus, we considered a fourth time delay distribution, a Gaussian distribution with fixed width ($\epsilon = 0.5$ Gyr) that allows either for positive or negative time delays:

$$(t; \epsilon) = \frac{1}{\epsilon \sqrt{2\pi}} e^{-\frac{(t-\epsilon)^2}{2\epsilon^2}} : \quad (9)$$

We also added a log-normal distribution, which is associated with processes where the source of uncertainty has multiplicative effects rather than additive ones, as is the case for Gaussian distributions. The best-fitting models to the theoretical time delays were in most cases log-normal distributions, whose width, in units of $\log(t)$, was kept fixed and determined by the best-fitting model of the theoretical time delays:

$$(t; \epsilon) = \frac{1}{\epsilon \sqrt{2\pi} \ln(\epsilon)^2} e^{-\frac{\ln(t-\epsilon)^2}{2 \ln(\epsilon)^2}} \frac{1}{t} : \quad (10)$$

The theoretical time delay distributions from Han & Podsiadlowski (2004) were also examined with a GOF test. They were produced assuming either the COWD + MS {SD scenario or the DD scenario with different binary evolution parameters. In Fig. 1 the theoretical time delay distributions of the SD and DD scenario together with two time delay distributions with different mean time delays are plotted, including the best-fitting model from S04.

2.5 The Star-Formation History (SFH)

Because we consider alternative prescriptions for the SFH that have incomplete redshift information, further complications arise. The ideal redshift coverage of the SFH should range from zero to the redshift of the first star formation, farther than the highest-redshift object presently known in the Universe. This is a consequence of the redshift range of the detected SNe and the long time delays that have to be considered. If high-redshift SNe only exploded after long time delays, their progenitors would need to form at redshifts up to $z \sim 30$, as Fig. 2 shows.

If the determination of the SFH did not cover the required redshift range, we used as an approximation either a

power-law extrapolation in time or a scaled version of the optical/UV derivation. We found that the method is not very sensitive to this approximation when the position of the peak of the SFH is well constrained, since it is the difference between the peaks of the SFH and the SNR that mainly constrains the best-fitting models. The alternative prescriptions of the SFH we have used are the following:

The SFH by Giavalisco et al. (2004), G04. We have used continuous approximations for the extinction corrected and not corrected models, inferred from deep optical/UV observations of galaxies in the GOODS field. Both versions differ by a factor of 3 in the redshift range of interest. The continuous approximations are the ones used in S04, which peak at $z \sim 2.7$ in the extinction corrected model (M1) and at $z \sim 1.8$ in the model that is not corrected for extinction (M2).

The best-fitting model of Chary & Elbaz (2001), hereafter CE01. It was derived from the integrated cosmic infrared background (CIRB) and covers the redshift range from 0 to 4.5. At $z > 4.5$ we tried a power-law extrapolation in time or a scaled version of G04 at $z > 3$. Mainly because the peak of the SFH occurs very late in time, at $z \sim 0.8$, we found that the inferred time delays are not very sensitive to this approximation. However, a constant SFH model is within the error bars at high z .

The SFH from Heavens et al. (2004), hereafter H04, inferred from the 'fossil record' of stellar populations in the Sloan Digital Sky Survey (SDSS). We interpolated a Spline function to the binned SFH, which peaks at $z \sim 0.4$, in order to obtain a smooth approximation. It is not usually recommended to approximate data in this way, but we think that our approximation preserves the general differences between this SFH and the alternative prescriptions. We also tried a scaled version of G04 at $z > 3$, or a constant star-formation history for all times, since this SFH is very flat at $z \sim 1$ and peaks very late in time with respect to the detected SNe. Both alternatives gave very similar results to the fit to the original binned data.

Additionally, we considered one of the most recent determinations of the SFH using Spitzer data, presented by (Perez-Gonzalez et al. 2005). However, both its limited redshift coverage and its dependence on the assumed galaxy luminosity function makes the high-redshift extrapolation ambiguous. For this reason, we did not try a continuous approximation of this SFH in the analysis, although it must be considered a reliable result. The variance between its different versions only demonstrates the persisting uncertainties in our knowledge of the SFH.

In Fig. 3 we show the four continuous approximations of the SFH and the binned SFH from PG05. The continuous approximations are based on the extinction corrected and not corrected SFH from G04, the best-fitting model from CE01 with a power-law extrapolation in time at high redshift and a continuous approximation of the best-fitting model from H04, which is constant at high redshift. It is apparent that there is a range of SFHs in the literature that do not agree and, importantly, peak at very different times. Thus, it is important to understand the systematic errors associated with this uncertainty. For a recent estimation of the uncertainties on the SFH see also Fig. 2 and 4 from Hopkins & Beacom (2006).

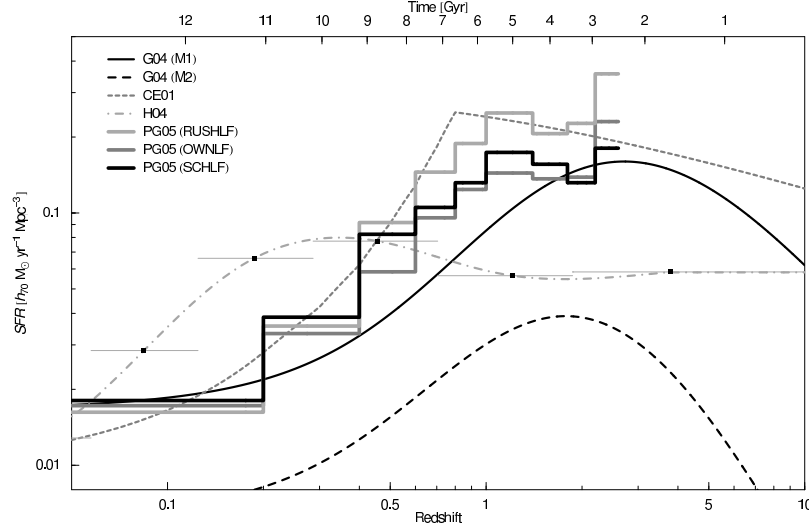


Figure 3. The alternative SFHs that better reflect the diversity of results obtained in the analysis. For G04 (Gavalis et al. 2004), M1 is the extinction corrected model and M2 is not corrected. For CE01 (Chary & Elbaz 2001), we used a power-law extrapolation in time for $z > 4.5$, but also a scaled version of G04 (not shown here), which gave very similar results. For H04 (Heavens et al. 2004), horizontal error bars represent bin sizes and vertical error bars (very small), bootstrap errors. In our calculations we chose to represent it by a smooth Spline interpolation. The PG05 (Perez-Gonzalez et al. 2005) SFHs are determined combining optical (UV data with Spitzer observations in the GOODS field, assuming different galaxy luminosity functions. The SNe in the Hubble Higher-z Supernova Search sample are in the redshift range from $z = 0.21$ to $z = 1.55$.

2.6 The Bayesian probability

Using Bayes theorem with a uniform prior, the probability of a mean time delay with a time-delay distribution (t_i) and a SFH in the form of $SFR(t_i)$, given the set of SN redshifts, fz_{ig} , is proportional to:

$$P(SFR(t_i); (t_i); fz_{ig}) \propto P(fz_{ig} | SFR(t_i); (t_i);) \quad (11)$$

Thus, it is proportional to the probability of the particular SN redshift distribution:

$$P(fz_{ig} | SFR(t_i); (t_i);) \propto \prod_{i=1}^N n_{Ia}(z_i;) \quad (12)$$

where $n_{Ia}(z;)$ has been normalised for every because the analysis is scale free. It depends on through the time-delay distributions of Section 2.4 and equations 1 and 2.

Hence, for a given combination of SFH, time-delay distribution and mean time delay, the predicted number of SNe per unit redshift can be expressed as a probability distribution in redshift. Subsequently, the probability of the set of SNe can be calculated for every .

2.7 New analysis

The main differences between the S04 calculations and this work are a result of considering a range of alternative SFHs. Further differences are as follows:

2.7.1 Redshift binning effects

The main advantage of using the observed redshift distribution of SNe Ia instead of the corresponding SNR (Gal-Yam

& Maoz 2004) is that the analysis can be done in a way that avoids binning and the subsequent loss of information.

Moreover, we have found that the analysis is very sensitive to the way the volume derivative is calculated in equation 2. Because the SN sample is small, binning the data is not recommended, and all the calculations should be done continuously. Binning can introduce a relative overestimation of the volume derivative at low redshift, effectively pushing the most probable time delays to higher values. As a result, the lower limit of the Bayesian analysis can be overestimated by more than 1 Gyr and the peak of the Bayesian probability distribution by 500 M yr, according to our calculations. This is consistent with the corrected results in Strolger et al. (2005b).

However, in order to get a continuous version of the control times we have used an interpolation of the values calculated in S04 at redshift intervals of 0.2. Recalculating the control times with more redshift resolution would be a better approach, but we have not tried it in this analysis.

2.7.2 Goodness of fit test (GoF)

A maximum likelihood analysis must be accompanied by a GoF test to check that the parametrized model has an appropriate form to start with, and only then can the confidence intervals be trusted at all. Accordingly, a χ^2 test was used to check consistency between the predicted and observed redshift histograms of SNe Ia in S04. However, the χ^2 test is not reliable when the number of elements per bin is not greater than five in 80 per cent of the bins (Will & Jenkins 2003). Instead, we have used a Kolmogorov-Smirnov test (KS test) as our goodness of fit test, which is the recommended test to use when the sample size is small and because the analysis is done continuously. Furthermore, se-

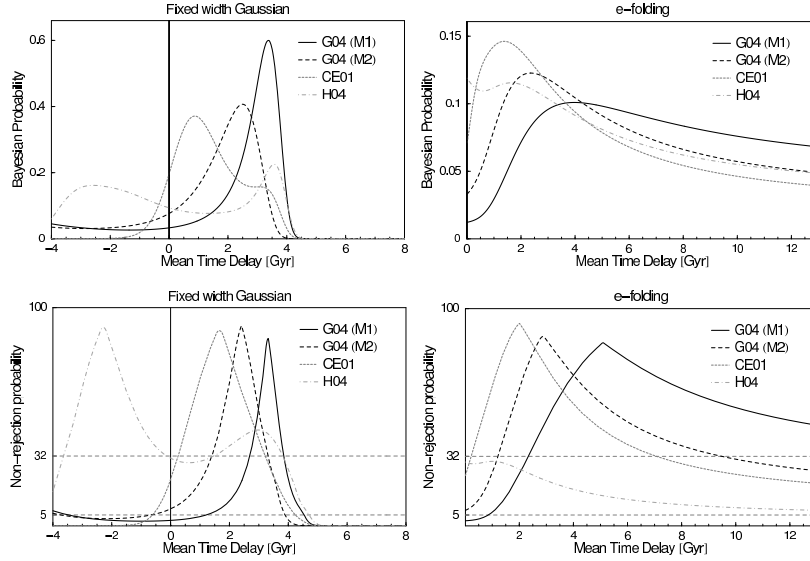


Figure 4. Bayesian probabilities and KS test non-rejection probabilities for the case of the ‘fixed width Gaussian’ and e-folding time delay distributions. The probabilities associated with the narrow Gaussian distribution are very similar to those associated with the ‘fixed width Gaussian’ distribution in the positive time-delay region. Note the relation between the most probable and best-fitting values with the peak of the SFHs in Fig. 3, i.e. later peaked SFHs give shorter time delays. The apparent preference for negative time delays in the case of the SFH from H04 may be an indication that this SFH peaks too late in time. See Section 3 for more details.

lecting the best-fitting models with the KS test can be used as an alternative parameter estimator.

2.7.3 Confidence intervals

In S04 the confidence intervals were obtained starting from the mode (the maximum) of the Bayesian probabilities, partly because in the original results the probabilities at low time delays were negligible. However, because in some cases the probability distributions are relatively flat, or not negligible at zero time delay, the definition of the confidence intervals becomes important. In our calculations, taking 95 per cent confidence intervals around the maximum vs. from the median can make a difference of typically 500 Myr.

One way to avoid this problem is to use the parameter region that is not rejected by the GOF test with a certain confidence level. In this approach, we obtain 95 and 68 per cent confidence intervals that are unambiguously defined.

2.7.4 Photometric redshifts

Because the spectra of SNe are characterised by many blended lines broadened by high velocity dispersion, SN redshifts are determined from their host galaxies. Of the 25 SNe Ia in the sample, six have only photometric redshifts, three of them in each field. We found that the photometric redshift of SN 2003al, 0.91 ± 0.02 , has a better estimate in the public COMBO-17 catalogue (Wolf et al. 2004) of 0.92 ± 0.04 . Additionally, in Strolger et al. (2005a), the photometric redshift of SN 2003lu, 0.11 ± 0.13 , has a better estimate of 0.14 ± 0.01 .

3 RESULTS

3.1 Varying the SFH

If alternative SFHs are allowed, the Bayesian probabilities associated with a given time-delay distribution have a wide range of preferred time delays. The Bayesian probabilities and KS test associated rejection probabilities show a preference for values ranging from very long (> 4 Gyr) to very short, and even negative (< -3 Gyr) if the SFH peaks very late in time (see Fig. 4). The relation between the peak of the SFH and the peak of the Bayesian probability distribution is, to zeroth order, such that later peaked SFHs give shorter time delays.

Interestingly, inspection of Fig. 4 (upper-left panel) shows two types of maxima in the Bayesian probabilities: one whose position decreases with later peaked SFHs and another that is fixed at approximately 3.5 Gyr, even for different SFHs. The first peak approximately reflects the time difference between the peaks of the SFH and the SNR. The second peak reflects the relative absence of SNe at high z . Because no SNe were detected between the epoch of reionisation and $z \approx 1.5$, or between $t \approx 0.5$ Gyr and $t \approx 4$ Gyr, the Bayesian analysis marginally favours models that do not produce SNe in the first 3.5 Gyr after the assumed epoch of reionisation. The upper plot of Fig. 2 is illustrative of this effect.

With the current data, it is the first peak which is statistically dominant for all the SFHs, but this may change with deeper and wider SN surveys in the future.

3.2 Kolmogorov-Smirnov test

With the KS test we find best-fitting mean time delays and confidence intervals that are free from the problems explained in Section 2.7.3. The rejection probabilities for the ‘fixed width Gaussian’ and e-folding time-delay distributions are shown in Fig. 4.

We found that all the combinations of SFH and time-delay distributions had an associated parameter region that is accepted by the KS test, which validates the use of the Bayesian analysis. Additionally, the parameter estimation seems robust in the sense that it gives results that are consistent with what the Bayesian analysis shows. Moreover, the addition of this test shows that the negative time-delay peak for the H04 SFH is favoured over the long time-delay peak (see Fig. 4), which may be an indication that this SFH is not compatible with the SN data.

3.3 Confidence intervals

The confidence intervals were defined as the parameter region that cannot be rejected with a certain confidence level based on the KS test. We found that only the extinction corrected SFH from Gialalisco et al. (2004) has a 95 per cent confidence lower limit greater than zero, i.e. around 1 Gyr. All the alternative SFHs did not result in a lower limit for the time delays greater than zero. A summary of the confidence intervals obtained with the Gaussian and e-folding time delay distributions is shown in Fig. 5.

3.4 Varying the time-delay distribution

The non-rejection regions of the five time-delay distributions tested in this work can be grouped into three families of results: one family associated with the 'fixed width Gaussian' (that allows for negative time delays) and 'narrow Gaussian' distributions, another with the 'wide Gaussian' and log-normal distributions and one associated with the e-folding distribution.

As a general rule, the narrower the test time-delay distribution, the narrower the associated Bayesian probabilities. However, it is in the long time-delay region where the changes are more noticeable, as can be seen in Fig. 5. This is because the abrupt transition that occurs in the SFH at the epoch of reionisation is reflected in a less smooth SNR when narrower time-delay distributions are assumed. Hence, the wider the time-delay distribution, the less pronounced the second peak in the Bayesian probabilities (see Section 3.1) and the longer the time delays allowed.

3.5 Theoretical time-delay distributions

We performed KS tests of the theoretical time-delay distribution varying the BPS parameters and the assumed SFHs. As a result, if the extinction corrected SFH from G04 is assumed, the $\text{COWD} + \text{MS} \{ \text{SD} \}$ scenario alone has a 3 per cent probability of not being rejected and the best-fitting models are obtained for a DD scenario which has a very high mass transfer efficiency. Conversely, if any of the theoretical models are assumed to be true, the best-fitting models are, in almost all the combinations, obtained with the SFH from Chary & Elbaz (2001). In Table 1 we show the non-rejection probabilities for the different combinations of SFH, theoretical scenario and BPS parameters tested in this work. The BPS parameters are: CE , the com ion (envelope ejection efficiency) efficiency as in Han & Podsiadlowski (2004); RLOF , the Roche lobe overflow mass transfer efficiency, and Z , the metallicity.

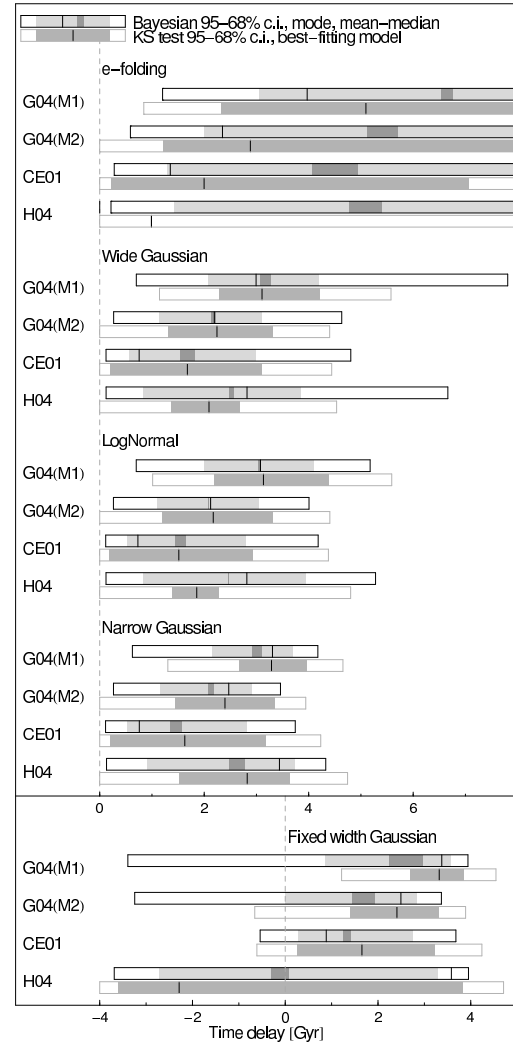


Figure 5. Summary of the parameter estimation analysis using different SFHs and alternative time-delay distributions. The Bayesian probability 95 and 68 per cent confidence intervals are plotted with the position of the mode and the mean (median interval), in addition to the KS test rejection probabilities 95 and 68 per cent confidence intervals and the position of the best-fitting time delay. Note that later peaked SFHs show a preference for shorter time delays and that wider time-delay distributions allow for longer time delays. H04 gives consistently poorer fits for positive time delays than for negative time delays as the use of the 'fixed width Gaussian' distribution shows (see Fig. 4 and the discussion in Section 2.4 for the use of negative time delays).

3.6 Constraints on the SFH assuming the theoretical models

In addition to the previous constraints on the time delay distribution we followed the approach of Gal-Yam & Maoz (2004) to constrain the SFH. The method assumes a particular time delay distribution and a SFH that consists of a broken power law smoothly joined at the transition redshift z_0 , proportional to $(1+z)$ at high z and to $(1+z)$ at low z , i.e.:

Table 1. Summary of the KS non-rejection probabilities (per cent) for different combinations of SFH, theoretical time-delay distribution and BPS parameters. Unless stated otherwise, the standard parameters are $\alpha_{CE} = 1.0$, $\alpha_{RLOF} = 1.0$ and $Z = 0.02$.

SFH	SD scenario { α_{CE} :			DD scenario { α_{CE} :		
	0.5	0.75	1.0	0.5	0.75	1.0
G 04 (M 1)	3.1	3.0	3.1	5.7	11.4	25.9
G 04 (M 2)	12.2	11.7	12.4	15.8	29.1	51.6
CE 01	49.8	47.8	50.8	48.1	69.2	85.4
H 04	28.1	28.1	28.0	25.7	24.2	21

SFH	DD scenario { Z :			DD scenario { α_{RLOF} :		
	0.001	0.004	0.02	0.5	0.75	1.0
G 04 (M 1)	11.0	13.2	25.9	25.9	47.4	56.5
G 04 (M 2)	30.1	31.2	51.6	51.6	82.6	78.5
CE 01	70.2	71.2	85.4	85.4	80.7	62.5
H 04	25.2	23.1	21.0	21.0	18.1	17.3

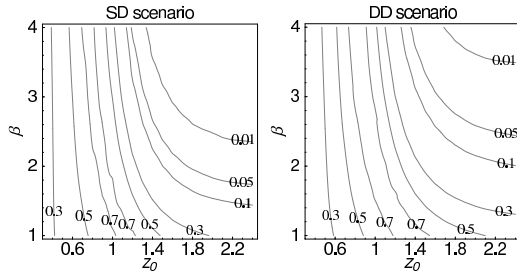


Figure 6. Constraints on the SFH assuming the theoretical time delay distributions. We show the KS test marginalised probabilities of not-rejecting a model with parameters z_0 and β (see equation 13). The probabilities are marginalised over β in the range -2 to 0 . We have also marginalised over z_0 and found that for the purpose of this work, the most important parameter is z_0 , followed by β and α in order of importance.

$$\text{SFR}(z) / \left(\frac{1+z_0}{1+z}^5 + \frac{1+z_0}{1+z}^5 \right)^{1-5} : \quad (13)$$

For more details see Gal-Yam & Maoz (2004). We assumed the theoretical time delay distributions and performed a KS test for different combinations of power-law indices and transition redshift, z_0 . We marginalised the probabilities on β because it was found that the dependency on this parameter is weak, which is expected because the SN sample contains very few objects at high redshift. The resulting probability distributions for different values of z_0 and β , assuming either the SD or DD scenario is shown in Fig. 6. Virtually all measurements of the SFH suggest $\text{SFR}(z) / (1+z)$, with β in the range -2 to 4 (Wilson et al. 2002; Perez-Gonzalez et al. 2005). For $\beta \geq 2$ we find that the peak of the SFH is most likely between $z = 0.7$ and 1.2 . However, any rejection at 90 per cent confidence is only possible for a peak location at $z \geq 2$. The latter the recent decline in the SFH (lower β), the less clearly constrained is the peak of the SFH.

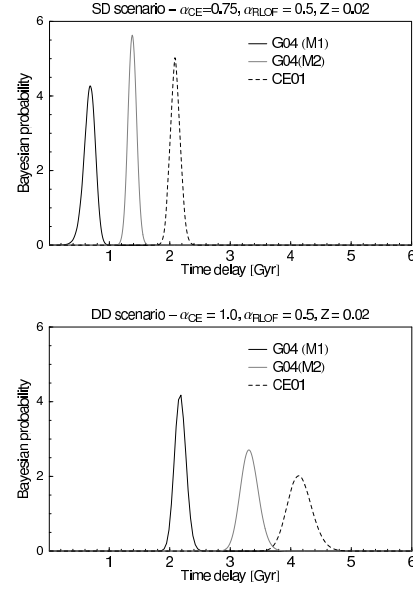


Figure 7. Systematic errors associated with the choice of SFH. We performed Monte Carlo simulations assuming two different SFHs: the labelled SFH to derive the mock sample of SNe, but the G 04 (M 1) SFH to derive the Bayesian probabilities. We show the Bayesian probabilities derived from 10,000 mock SNe for one combination of BPS parameters in the SD and DD scenarios, respectively. The associated systematic error are of the order of 2 Gyr.

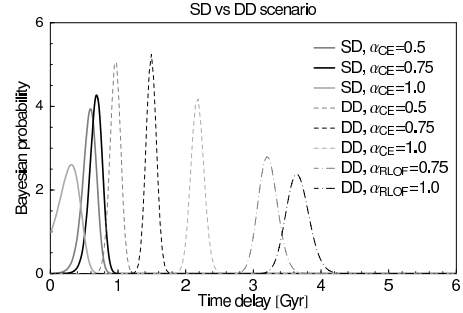


Figure 8. Systematic errors associated with the choice of BPS parameters. The G 04 (M 1) SFH is assumed and the BPS parameters are changed. Because the time delay distribution are not fully sampled, the mean time delays are underestimated in some cases, but by less than 0.5 Gyr. If some BPS parameters are changed, differences of up to $\sim 3-4$ Gyr are found for the mean time delay of the DD scenario, while for the SD scenario they are of the order of ~ 0.5 Gyr.

4 MONTE CARLO SIMULATIONS

In this section we examine whether our approach is subject to systematic biases due to the method itself and the choice of the SFH.

To assess the robustness of the method, we performed Monte Carlo simulations for each progenitor scenario separately, where we took large sets of simulated SNe (typically 10,000) to minimize statistical errors. Because the DD scenario can extend to times comparable to the age of the universe, its time delay distribution cannot be sampled completely; we therefore expect that the recovered values will always be biased towards shorter mean time delays. We found

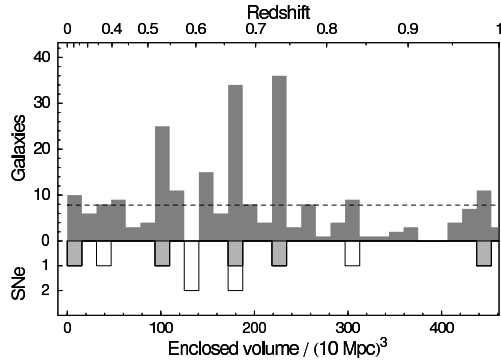


Figure 9. Redshift histogram of a complete sample of galaxies in the GOODS (Southern field from the VVDS survey (gray), all the SNe with spectroscopic redshift in the field (white) and only the SNe Ia with spectroscopic redshift (light gray). Bins are chosen to show constant comoving volume. The dashed line shows the average galaxy density (assuming no evolution). Several peaks are due to large-scale structure. Note that at higher redshifts the width of structures appears artificially enhanced by the distorted redshift scale.

the following: (1) such an expected bias is indeed present for the DD scenario, but is always below 0.5 Gyr; (2) for large sample sizes, the smallest statistical errors are obtained using the e-folding time delay distribution, independent of the theoretical scenario assumed.

To quantitatively estimate the systematic errors associated with the choice of SFH, we proceeded in the following way: (1) in order to minimize the statistical errors and study the systematics, we performed Monte Carlo simulations with 10,000 mock SNe drawn from the theoretical scenarios, using the e-folding time-delay distribution in the analysis; (2) we produce a mock sample of SNe with a SFH that differs from the one used in the Bayesian analysis; (3) a comparison between the different recovered mean time delays then gives an estimate of the systematic error due to the choice of SFH (see Fig. 7 and Fig. 8). The result is consistent with what can be concluded from Section 3, i.e. that the bias on the mean time delay can be of the order of 2 Gyr, even ignoring the H04 SFH.

We then tested the robustness of the algorithm with small samples. In order to do this, we performed Monte Carlo simulations with 10,000 different sets of 25 mock SNe drawn from the theoretical models. We repeated the Bayesian and GoF analysis and found the following: (1) when the theoretical time delays are relatively short and the SFH peaks early in time, or when the time delays are long and the SFH peaks late in time, the Bayesian probabilities tend to have very positive or very negative skewness and, consequently, the mode of the Bayesian probabilities either overestimates or underestimates the theoretical mean time delays; (2) the distribution of non-rejection probabilities using the KS test is flat, meaning that there is no significant bias towards short or long time delays. Hence, we conclude that the mode of the Bayesian probability is not a good estimator for the mean time delays, while the KS test confidence intervals are robust even with small samples, general results consistent with the discussion in Press et al. (1992).

5 DISCUSSION

5.1 Large scale structure

Large-scale structure (LSS) effects are important in small pencil beam surveys when studying the time delay of SNe Ia, even when the SFH and the SNR have been measured in the same field. Usually, the SFR is measured as an ‘instantaneous’ observed rate at a particular location in space and time, where for this study a prediction of the SNR will be needed for comparison. However, this prediction ought to be based on the SFR in the same position in space, not only at the time when the SNe are seen to explode, but at earlier times as well.

Since the latter figure can not be measured directly, we have to obtain the SFR for earlier times by looking at a higher redshift, i.e. at a different location in space. Cosmic variance and the dependence of star formation on local environment will lead to a SFR measurement that is somewhat different from the past SFR of the target location in the same field. This SFR variance will appear whether the SFR is measured from the same fields or not, since the locations in space where the SFR and SNR are measured will be unrelated. A 1 Gyr time delay already translates into proper distance differences of 500 Mpc at $z = 1$.

So, if we do not know the individual star-formation histories of galaxies in the supernova field, we are best advised to use our best knowledge of the cosmic SFH, while LSS still leaves an imprint on the observed SNR history. We investigate the large scale structure in the CDFS where the spectroscopic redshift survey VIMOS VLT Deep Survey (LeFevre et al. 2004, VVDS) overlaps almost precisely with the GOODS field and is complete to $M_V < -19.5$ at $z < 1$. In Fig. 9 we show a histogram of galaxy redshifts with $M_V < -19.5$ in bin sizes chosen to contain a constant comoving volume of $(25 \text{ Mpc})^3$. A non-evolving and homogeneous galaxy distribution should appear flat in this representation. Well-known over-densities or wall-like structures are clearly apparent, especially in the redshift range from 0.5 to 0.75. Two wall-like structures near $z = 0.67$ and $z = 0.74$ are conspicuous in the distribution and have been observed in both x-ray and optical surveys (see e.g. Gilli et al. 2003; Wolf et al. 2004, for independent confirmation).

Also shown is a histogram of SNe Ia with secure (spectroscopic) redshift determinations. SNe with photo- z ’s only have been omitted due to the large error in redshift which makes any association with structures in the galaxy distribution difficult.

The average bin in the redshift range from 0 to 1 contains 7.8 galaxies, whereas the average SNe-weighted bin contains 16.7 galaxies (2.14 times the normal average), a possible indication that the inferred SNR is affected by LSS in this field and redshift range. In order to understand how these numbers depend on the choice of our bins, we have repeated the calculations for bin widths of $(\Delta V)^{1/3} = (20; 21; 25) \text{ Mpc}$ and found ratios of 2.52, 2.38, 2.15, 2.22, 2.00 and 2.14, respectively. Interestingly, the ratios that result using only SNe Ia-weighted bins are even higher: 2.87, 2.68, 2.88, 3.29, 2.55 and 2.97.

The imprint of LSS in the SNR distribution could be corrected in the analysis of time delays. If the underlying mass density on a given direction \hat{n} were of the form $\langle \delta(z) \rangle = \bar{\delta}(z)(1 + \langle \delta(\hat{n}; z) \rangle)$, the over-densities could be cor-

rected by multiplying the control times by the same factor, $1 + \langle \dot{m} \rangle / \langle \dot{m}_0 \rangle$. However, we do not correct for density variations, because we lack a good determination of the LSS with consistent quality in both fields.

5.2 SN rates and efficiencies

In the process of matching the observed number of SNe with a model, it is possible to explicitly calculate the SN production efficiencies and the supernova rate (SNR). Not only does the shape of the SNR history constrain the progenitor models via the delay times, but also the SN efficiency must be compatible with the model.

As a first consistency test, we compare the directly measured SNR with the parametrized estimates. In Fig. 10 we show two versions using the results of the parameter estimation with the G04 (M1) and CE01 SFHs. Clearly, the extinction corrected SFH from G04 with the narrow Gaussian distribution is consistent with long time delays (~ 3.5 Gyr), whereas the SFH from CE01 matches best with an e-folding distribution of shorter time delays (~ 1.5 Gyr). The second alternative is only marginally favoured by the KS test, so both possibilities seem equally plausible.

It is important to mention that in Strolger et al. (2005a) a deeper SN search in the smaller Ultra Deep Field and its parallel fields (UDF/P) resulted in the detection of four additional SNe with $z < 1.4$. The lack of high-redshift SNe is one of the predictions of the S04 best-fitting model and hence it supports the result. However, the authors also considered the SFH from CE01, but without any time delay, and concluded that it is not possible to rule out this SFH with more than 50 per cent confidence.

The SN efficiencies required to explain the observed SNR pose a problem for the theoretical SD scenario, which produces too few SNe. This is true for all SFHs and combination of parameters, and amounts to a shortfall of 4 to 10 depending on the assumed SFH. The DD scenario can reproduce the required efficiencies for some combinations of BPS parameters. However, changes in the little constrained binary fraction and mass ratio distributions, or possibly in the initial mass function (IMF), may solve this problem in the future.

One additional challenge is that the time-delay distribution or the supernova efficiencies may evolve with time: if the delay distribution is made up of several components from different SN production channels, their relative contribution could change with time; the supernova efficiencies themselves may evolve with time, especially considering that the accretion processes could depend on environmental factors such as the metallicity (Kobayashi et al. 1998). The relative absence of SNe at high redshift could be a result of a metallicity effect, rather than a reflection of the time delays. If this is truly the case, our error bars on the time delays would be largely underestimated. The use of compatible star formation and chemical enrichment histories will be required to tackle this problem.

5.3 Spitzer SFH

We have shown that it is crucial to determine the SFH that is to be used in the analysis. The recent determination of the

SFH from Perez-Gonzalez et al. (2005), using three different extrapolations of the galaxy luminosity function, was shown in Fig. 3. This SFH was obtained by combining infrared Spitzer observations with optical/UV data of galaxies in the GOODS field. The resemblance between this SFH and the CE01 best-fitting model justifies the use of the latter.

Interestingly, the recent near-infrared and submillimetric determination of the SFH from Wang, Cowie & Barger (2005) peaks at $z \sim 1$, similarly to what is obtained in CE01. These new results emphasize the persistent uncertainties in our knowledge of the SFH and the problem of extinction corrections in the optical.

6 CONCLUSIONS

We have found that systematic errors associated with the use of alternative star-formation histories are comparable if not larger than the statistical errors reported in Strolger et al. (2004). The position of the peak of the SFH was found to be the crucial parameter for the recovered time delays: Later peaked SFHs result in lower time delays and vice versa. Furthermore, the confidence intervals for the time delays depend on the functional form of the delay distributions assumed in the analysis. The use of wider time-delay distributions, in particular the e-folding model, gives considerably longer upper limits for the time delays.

For the data set under investigation, we found that the KS test is better suited to obtain confidence intervals than a Bayesian analysis. The KS test confidence intervals are unambiguously defined, and we have confirmed their validity using Monte Carlo simulations. In contrast, the skewness of the Bayesian probabilities and the small sample size result in somewhat arbitrary confidence intervals.

A KS test using the shape of the theoretical time-delay distributions shows that the extinction corrected model from G04 is incompatible with the COWD + MS {SD scenario, although other SFHs are compatible. The DD scenario cannot be rejected at 95 per cent confidence with any combination of SFH and time-delay distribution. Starting from theoretical time-delay distributions, they consistently favour the SFH from CE01.

If we wish to constrain the time-delay distribution and possibly discard progenitor scenarios from the redshift distribution of supernovae, it is of foremost importance to determine the cosmic star-formation history more accurately. Otherwise, the uncertainty in the SFH will continue to limit the interpretation of SN data sets of any conceivable size.

Secondly, we would need a better understanding of our progenitor models: if we ignore factors affecting efficiencies, their cosmic evolution will make the delay time distributions evolve and produce a situation where it is hard to disentangle these different effects without qualitatively different observations.

Only after having solved these issues would deeper and wider surveys help to constrain the delay times and progenitor models by decreasing statistical noise and reducing the influence of environmental cosmic variance on the supernova samples.

Different observations have already produced some evidence for shorter time delays: Recent work by Mannucci et al. (2005) showed that the most efficient host galaxies

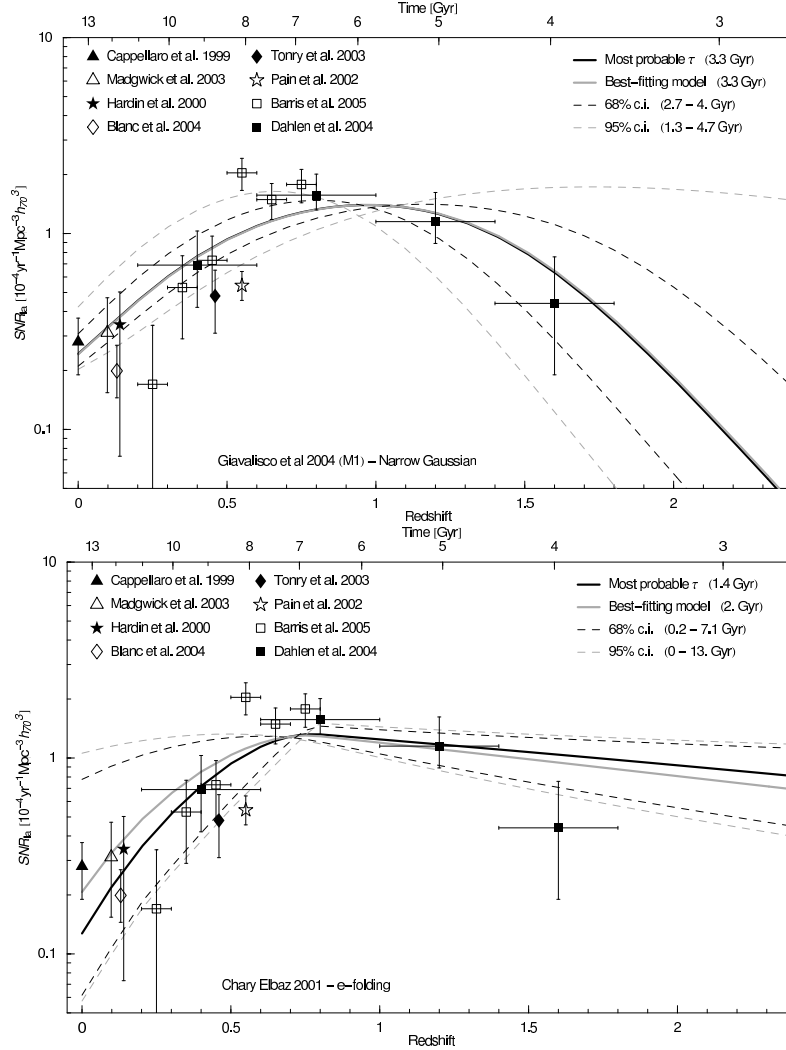


Figure 10. Determinations of the SNR in the literature compared with the parameterized versions used in the analysis. The most probable corresponds to the mode of the Bayesian probabilities and the best-fitting model corresponds to the model with the smallest KS test D value. The confidence intervals are based on the KS test, corresponding to the models where the non-rejection probabilities are 0.32 and 0.05, for the 68 and 95 per cent confidence intervals, respectively. The horizontal error bars are the bin sizes in Dahlen et al. (2004) and Barris & Tonry (2005). Note that the highest redshift bin from Dahlen et al. (2004) is based on two detected SNe. The best-fitting models and confidence intervals are obtained using only the SN sample from S04.

for SNe Ia production among all galaxies are irregulars, and Della Valle et al. (2005) showed that among elliptical galaxies it is in particular the radio-loud galaxies, which are also believed to be associated with recent star formation. Also, (Gamavich & Gallagher 2005) have shown that SNe Ia of normal luminosity occur particularly in those elliptical galaxies with quite substantial star-formation rates. Also, SNe Ia in galaxy clusters seem to indicate time delays that are shorter than 2 Gyr (Maoz & Gal-Yam 2004).

Finally, it is clear that, if the SNe Ia phenomenon is composed of several production channels, all conclusions we have drawn apply to the dominant channel. A generally less common channel with different characteristics could again be the dominant channel in a subset of galaxies with older-age or higher-metallicity stellar populations. It is already established that under-luminous 91bg-type SNe Ia preferably occur in non-star-forming hosts, such as ellipticals. It remains to be explored theoretically, whether the COWD +

RG {SD scenario could be related specially to old populations. We should also consider the possibility that we may not even have found the dominant progenitor channel for normal SNe Ia (Hamuy 2003; Tout 2005).

Even if the SFH peaks at redshift $z \approx 1$ and the recovered time delays are consequently low, the associated SNR (see Fig. 10, lower panel) tends to be over-estimated in the highest- z bin. This effect could be interpreted as the signature of a long time delay component that does not contribute to the total SNR when the universe is too young. However, because the highest- z bin only contains two SNe, this does not lead to low non-rejection probabilities. A study of bimodal time delay distributions could only be done with this method if the uncertainties in the SFH were significantly reduced and the metallicity cut on the efficiencies was properly quantified.

If different channels produce SNe Ia from progenitors of distinctly different age or metallicity, then an increase of

the supernova sample could greatly help the identification of the various plausible progenitors. However, such a dataset would most be beneficial if it is complemented with host galaxy characterisation (see van den Bergh, Li & Filippenko 2005) and spectra with better signal (see Benetti et al. 2005).

ACKNOWLEDGMENTS

We are indebted to Louis-G. Strolger for fruitful discussions and providing us with the control times required in the analysis. We also thank Guillaume Blanc, Ranga-Ram Chary, Ben Panther, Alan Heavens and Pablo Perez-Gonzalez for discussions related to the SFH and Klaus Meisenheimer and an anonymous referee for comments that significantly improved the manuscript. F.F. was supported by a Fundación Andes (PPARC Gemini) studentship. C.W. was supported by a PPARC Advanced Fellowship. This work was in part supported by a Royal Society UK-China Joint Project Grant (Ph.P. and Z.H.), the Chinese National Science Foundation under Grant Nos. 10521001 and 10433030 (Z.H.) and a European Research & Training Network on Type Ia Supernovae (HPRN-CT-20002-00303).

REFERENCES

- Barris B. J. & Tonry J. L., 2005, *arXiv astro-ph/0509655*, accepted in *ApJ*.
- Benetti S. et al., 2005, *ApJ*, 623, 1011
- Blanc G., et al. 2004, *A & A*, 423, 881
- Cappellaro, E., Evans, R., Turatto, M. 1999, *A & A*, 351, 459
- Chary R., Elbaz D., 2001, *ApJ*, 556, 562
- Dahlen T. et al., 2004, *ApJ*, 613, 189
- Della Valle M., Panagia N., Padovani P., Cappellaro E., Mannucci F., Turatto M., 2005, *ApJ*, 629, 750
- Gal-Yam A., Maoz D., 2004, *MNRAS*, 347, 942
- Gamazo V. N., Khokhlov A. M., Olan E. S., 2005, *ApJ*, 623, 337
- Gamovich P. M., Gallagher J., 2005, *arXiv astro-ph/0501065*
- Giazalisco M. et al., 2004, *ApJ*, 600, L103
- Gilli R., et al. 2003, *ApJ*, 592, 721
- Hardin D., et al. 2000, *A & A*, 362, 419
- Hachisu I., Kato M., Nomoto K., 1996, *ApJ*, 470, L97
- Hachisu I., Kato M., Nomoto K., 1999, *ApJ*, 522, 487
- Hamuy M. et al., 2003, *Nat*, 424, 651
- Han Z., Podsiadlowski P., 2004, *MNRAS*, 350, 1301
- Heavens A., Panter B., Jimenez R., Dunlop J., 2004, *Nat*, 428, 625
- Hillebrandt W., Niemeyer J. C., 2000, *ARA & A*, 38, 191
- Hopkins A. M., Beacom J. F., 2006, *arXiv astro-ph/0601463*, submitted to *ApJ*.
- Iben I., Tutukov A. V., 1984, *ApJS*, 54, 335
- Kobayashi C., Tsujimoto T., Nomoto K., Hachisu I., Kato M., 1998, *ApJ*, 503L, 155K
- Langer N., Deutschmann A., Wellstein S., Hönig P., 2000, *A & A*, 362, 1046
- Le Fevre O., et al. 2004, *A & A*, 428, 1043
- Li X.-D., van den Heuvel E. P. J., 1997, *A & A*, 322, L9
- Mannucci F., della Valle M., Panagia N., Cappellaro E., Cresci G., Maiolino R., Petrosian A., Turatto M., 2005, *A & A*, 433, 807
- Maoz D., Gal-Yam A., 2004, *MNRAS*, 347, 951
- Madgwick D. S., Hewett P. C., Mortlock D. J., & Wang L., 2003, *ApJ*, 599, L33
- Nomoto K., Iben I., 1985, *ApJ*, 297, 531
- Nomoto K., Kondo Y., 1991, *ApJ*, 367, L19
- Pain R., et al. 2002, *ApJ*, 577, 120
- Perez-Gonzalez P. G., Rieke G. H., Egami E., et al., 2005, *ApJ*, 630, 82
- Perlmutter S. et al., 1999, *ApJ*, 517, 565
- Phillips M. M., 1993, *ApJ*, 413, L105
- Press W. H., Teukolsky S. A., Vetterling W. T., & Flannery B. P. 1992, *Numerical recipes in C: The art of scientific computing*, Cambridge University Press
- Rappaport S., DiStefano R., Smith J. D., 1994, *ApJ*, 426, 692
- Riess A. G. et al., 1998, *AJ*, 116, 1009
- Riess A. G. et al., 2004, *ApJ*, 607, 665
- Ropke F. K., Hillebrandt W., 2005, *A & A*, 431, 635
- Saio H., Nomoto K., 1985, *A & A*, 150, L21
- Saio H., Nomoto K., 1998, *ApJ*, 500, 388
- Shapiro S. L., Teukolsky S. A., *Black holes, white dwarfs and neutron stars: The physics of compact objects*
- Strolger L.-G. et al., 2004, *ApJ*, 613, 200
- Strolger L.-G. & Riess A. G., 2005, *arXiv astro-ph/0503093*, submitted to *AJ*.
- Strolger L.-G., et al. 2005, *ApJ*, 635, 1370
- Timmes F. X., Woosley S. E., Taam R. E., 1994, *ApJ*, 420, 348
- Tonry J. L., et al. 2003, *ApJ*, 594, 1
- Tout C. A., 2005, *ASPC*, 330, 279
- van den Heuvel E. P. J., Bhattacharya D., Nomoto K., Rappaport S. A., 1992, *A & A*, 262, 97
- van den Bergh S., Li W., Filippenko A. V., 2005, *PASP*, 117, 773
- Wall J. V., Jenkins C. R., 2003, *Practical Statistics for Astronomers*, Cambridge University Press
- Wang W. H., Cowie L. L. and Barger A. J., 2005, *arXiv astro-ph/0512347*, submitted to *ApJ*.
- Webbink R. F., 1984, *ApJ*, 277, 355
- Wilson G., Cowie L. L., Barger A. J., Burke D. J. 2002, *AJ*, 124, 1258
- Wolf C., Meisenheimer K., Kleinheinrich M., et al., 2004, *A & A*, 421, 913